Atmos. Meas. Tech. Discuss., 7, 233–255, 2014
www.atmos-meas-tech-discuss.net/7/233/2014/
doi:10.5194/amtd-7-233-2014

Atmospheric Measurement Techniques Discussions

Intercomparison of Hantzsch and fiber-laser-induced-fluorescence formaldehyde measurements

J. Kaiser[1], X. Li[2], R. Tillmann[2], I. Acir[2], F. Rohrer[2], R. Wegener[2], and F. N. Keutsch[1]

[1]Department of Chemistry, University of Wisconsin-Madison, Madison, WI, USA
[2]Institut für Energie- und Klimaforschung, Troposphäre (IEK-8), Forschungszentrum Jülich, Jülich, Germany

Received: 17 December 2013 – Accepted: 20 December 2013 – Published: 14 January 2014

Correspondence to: J. Kaiser (jen.b.kaiser@gmail.com)

Published by Copernicus Publications on behalf of the European Geosciences Union.

Abstract

Two gas-phase formaldehyde (HCHO) measurement techniques, a modified commercial wet-chemical instrument based on Hantzsch Fluorimetry and a custom-built instrument based on Fiber-Laser Induced Fluorescence (FILIF), were deployed at the atmospheric simulation chamber SAPHIR to compare the instruments' performances under a range of conditions. Thermolysis of para-HCHO and ozonolysis of 1-butene were used as HCHO sources, allowing for calculations of theoretical HCHO mixing ratios. Calculated HCHO mixing ratios are compared to measurements, and the two measurements are also compared. Experiments were repeated under dry and humid conditions (RH < 2 % and RH > 60 %) to investigate the possibility of a water artifact in the FILIF measurements. The ozonolysis of 1-butene also allowed for the investigation of an ozone artifact seen in some Hantzsch measurements in previous intercomparisons. Results show that under all conditions the two techniques are well correlated ($R^2 \geq 0.997$), and linear regression statistics show measurements agree with within stated uncertainty (15 % FILIF + 5 % Hantzsch). No water or ozone artifacts are identified.

1 Introduction

Typical tropospheric formaldehyde (HCHO) concentrations range from 100 ppt in remote polar regions to 20 ppb in urban areas (e.g. Sumner et al., 2002; Dasgupta et al., 2005). Sources of HCHO include primary emissions from anthropogenic activities, biomass burning, and importantly, the oxidation of anthropogenic and biogenic volatile organic compounds (VOCs). The oxidation of VOCs is linked to the formation of secondary pollutants such as secondary organic aerosol and ozone (O_3). Not only is HCHO a product of VOC oxidation, but it also is a major source of the HO_x ($HO_x = OH + HO_2$) radicals that drive the atmosphere's oxidative capacity (Seinfeld and

AMTD
7, 233–255, 2014

Pandis, 2006). Accurate and precise measurements of HCHO are therefore necessary to test models of the oxidation mechanisms that form secondary pollutants.

Several measurement techniques for detection of atmospheric HCHO have been developed. These include solution-phase chemical techniques such as 2,4-dinitrophenylhydrazine (DNPH) derivatization followed by gas chromatography or high pressure liquid chromatography, the coil enzyme (CENZ) fluorometric method, and Hantzsch derivatization followed by fluorimetry (Heard, 2006, and references therein). In efforts to improve time resolution and avoid the scrubbing process, spectroscopic techniques such as Fourier transform infrared spectroscopy (FTIR), differential optical absorption spectroscopy (DOAS), tunable diode laser absorption spectroscopy (TDLAS), and laser induced fluorescence (LIF) have also been developed (Heard, 2006, and references therein; Hottle et al., 2009). When corrected for humidity effects, proton-transfer mass spectrometry (PTR-MS) has also shown to be a promising method for ambient HCHO measurements (Warneke et al., 2011).

Recently, a formal blind intercomparison between BB-DOAS, DNPH-HPLC, PTR-MS, and two Hantzsch instruments was performed at the atmospheric simulation chamber SAPHIR (Simulation of Atmospheric PHotochemistry In a large Reaction Chamber) (Wisthaler et al., 2008). Aside from a few reported analytical issues, the agreement between all four techniques was reported as fair. Notably, one Hantzsch instrument (Methanalyser, Alpha Omega Power Technologies, Model MA-100, Albuquerque, New Mexico, USA) equipped with a modified inlet was affected by a non-constant offset. It was further concluded that a different Hantzsch instrument (AL4021, Aerolaser GmbH, Garmisch-Partenkirchen, Germany) was affected by a negative ozone bias during part of the intercomparison.

A recent intercomparison between a Hantzsch instrument built in-house and a commercial PTR-MS (IoniconAnalytik GmbH, Innsbruck, Austria) at a rural site in Ontario found the two techniques agreed within 5 % (Vlasenko, et al., 2010). Significant scatter for mixing ratios below 1.5 ppb was observed, but not attributed to either technique specifically.

AMTD
7, 233–255, 2014

While the FIber Laser-Induced Fluorescence (FILIF) instrument has been deployed on several field campaigns (e.g. DiGangiet al., 2011; DiGangiet al., 2012; Ahlm et al., 2012; Liet al., 2014), it has only been compared with a time of flight proton-transfer mass spectrometer (PTR-TOF-MS) during the BEACHON-ROCHS field study in the summer of 2010 (Kaser et al., 2013). For both instruments, a large uncertainty of 30–50 % is reported. While the two measurements were well correlated ($R^2 = 0.72$), the FILIF measurements were a factor of 2 less than PTR-TOF-MS measurements. Authors note PTR-TOF-MS measurements provide an upper limit of formaldehyde mixing ratios, as interferences may occur from species which fragment to m/z 31.0177. However, the largest uncertainty was attributed to calibration methods that were not cross calibrated.

To better understand the poor agreement between PTR-TOF-MS and FILIF measurements at BEACHON, a Hantzsch instrument and FILIF were deployed at the SAPHIR chamber for a four-part intercomparison. The same FILIF calibration source was used during this intercomparison and the BEACHON campaign to minimize instrumental differences between the two studies. As Hantzsch measurements have been shown to agree well with spectroscopic techniques and PTR-MS, a comparison between FILIF and Hantzsch provides a secondary check on the accuracy of the FILIF technique. Furthermore, controlled chamber settings allow for calculation of theoretical HCHO mixing ratios, providing another assessment of instrument accuracy.

An additional goal of the intercomparison was to examine the possibility of a water vapor artifact for FILIF. As water quenches fluorescence more efficiently than nitrogen, the theoretical sensitivity of FILIF is lower under high relative humidity (RH). Indeed, other fluorescence-based measurements apply an RH-dependent calibration to correct for this difference in observed fluorescence signal due to higher quenching (e.g. Schlosser et al., 2009). Laboratory RH-dependent calibrations have shown no observable effect of H_2O on FILIF sensitivity (DiGangi et al., 2012). These calibration calculations are limited by the assumption that the water used to humidify the airstream contains no dissolved HCHO. By comparing the Hantzsch and FILIF measurements under

AMTD
7, 233–255, 2014

low and high RH conditions, the assumption that any RH-dependence is negligible can be tested. Furthermore, by using two sources of formaldehyde in the SAPHIR chamber, either thermolysis of para-HCHO or ozonolysis of 1-butene, the previous ozone artifact seen in some Hantzsch measurements can be assessed.

2 Instrument descriptions

2.1 Fiber-laser induced fluorescence

The FILIF instrument has been described in detail elsewhere (Hottle et al., 2009; DiGangi et al., 2011), but will be briefly discussed here. The beam from a 20 mW, 353 nm tunable, pulsed, narrow-bandwidth laser (NovaWave Technologies,TFL Series) is directed into a 32-pass White-type cell. The resulting fluorescence from HCHO from 390 to 500 nm is focused into a photomultiplier tube. The output beam from the White cell is directed into a glass cell containing high concentrations of gas phase HCHO for wavelength reference. The laser wavelength was scanned over the fluorescence feature every 90 s, and the laser was dithered on and off the rovibronic absorption line for 700 ms and 300 ms, respectively. The HCHO mixing ratio is proportional to the difference between the fluorescence signal observed when the laser is on and off the absorption feature, as well as the laser power.

FILIF calibrations were performed for each experiment using a HCHO permeation tube (VICI Metronics, 100-044-2300-U45) heated to 85 °C in a portable calibration gas generator (VICI Metronics, Model 120). The permeation source has been characterized using Fourier Transform Infrared spectroscopy, as described elsewhere (DiGangi et al., 2011). A spectral feature different from the feature used during the rest of the campaign was used on the first day of the intercomparison, resulting in a 5 % larger sensitivity for this day.

During the intercomparison, 1σ precision derived from measurements of synthetic air was ~ 20 ppt in 1 s. Above 3 ppb, precision is a function of the observed signal derived

AMTD
7, 233–255, 2014

from the standard deviation of the measurement at a constant concentration. Accuracy was 15 % as limited by the permeation tube calibration. Calibrations were performed up to concentrations of 4 ppb, and linear extrapolation was assumed for higher concentrations. This linearity assumption was verified in later lab-based experiments in which successive dilutions of a concentrated HCHO standard (Scott Marrin, ~ 11 ppm) in synthetic air were measured. The linear fit of signal to concentration in the 0–4 ppb range was not statistically different from the fit over the entire concentration range (0–20 ppb).

Chamber air was sampled at 6 L min^{-1} through ~ 10 m of 4 mm I.D. PFA Teflon tubing and a 5 µm Teflon particle filter. Previous studies have shown inlet effects for configurations of this nature are negligible (Wert et al., 2002). Instrument zeros performed by overflowing the inlet either with or without the particle filter and tubing agreed within 30 ppt. In contrast to previous deployments of this instrument, sample air was used both as the bulk flow through the White cell and to purge the volumes of the white cell not in the detection volume.

During the intercomparison, uncharacteristically rapid and large fluctuations in laser power and wavelength were observed, adding high uncertainty to FILIF measurements. This data is excluded from the analysis, as it does not reflect typical in-field operations of the FILIF instrument.

2.2 Hantzsch Fluorimetry

HCHO measurement by Hantzsch Fluorimetry was performed by a modified commercial instrument (AL4001, Aerolaser GmbH, Germany) (Kelly and Fortune, 1994). At a controlled flow rate of 1 L min^{-1}, the chamber air is sampled through a $L = 10$ m, O.D. = 1/4″ PFA tube into a temperature controlled (12 ± 0.2 °C) stainless steel stripping coil. In addition, a stripping solution of 0.05 mol L^{-1} H_2SO_4 is continuously pumped through the coil at a flow rate of 0.35 mL min^{-1}. The liquid flow is continuously monitored by a flow meter (LFM). HCHO in the sampled air is stripped into the liquid phase with an efficiency of 98 % (Krinke, 1999). The formed HCHO solution is then separated from the gas phase and continuously mixed with a Hantzsch reagent (5.6 mol L^{-1}

AMTD
7, 233–255, 2014

Ammonium Acetate, 0.16 mol L^{-1} Acetic Acid, and 0.02 mol L^{-1} Acetylacetone). In a continuous flow reactor held at 70 °C, HCHO reacts with the Hantzsch reagent forming the dye 3,5-diacetyl-1,4-dihydrolutidine. The dye solution is then illuminated by a phosphor coated mercury lamp. The emitted fluorescence signal is detected by a photomultiplier at 510 nm.

The sensitivity of the instrument is calibrated using liquid HCHO standards. The standards are added to the stripping coil instead of the stripping solution while HCHO-free air is passed through the coil. The calibration is performed at 3 concentration levels of liquid HCHO standards. The concentrations correspond to gas phase mixing ratios of 2 ppb, 10 ppb, and 35 ppb. HCHO-free air is generated by passing the sampled air through a catalyst (Hopkalit, Draeger) at room temperature. The HCHO-free air is also used to determine the background signal of the instrument. During the campaign, the Hantzsch instrument was placed in one of the containers below the SAPHIR chamber. The ambient temperature inside the container was kept at 23 °C. Calibrations for the sensitivity of the instrument, as well as for the measured flow rates were performed in the beginning and in the end of the campaign. The determined sensitivities of the instrument differs less than 2 %. The accuracy of the Hantzsch measurements was around 5 %, stemming mainly from the uncertainty of the calibration. The 1σ precision derived from the HCHO-free air measurements was around 25 ppt in 11 s. The data is recorded every 11 s as a 2 min running average.

2.3 Supporting instrumentation

In addition to the HCHO instruments, several additional measurements were recorded during the intercomparison. A summary of the supporting measurements is provided in Table 1.

Notably, C_4H_8 measurements were provided in arbitrary units. C_4H_8 concentrations used in this analysis were calculated from the known amount of C_4H_8 injected and the maximum observed counts. When H_2O mixing ratio measurements were unavailable,

AMTD
7, 233–255, 2014

values were calculated from the measured dew point and the observed temperature. During the third day, data from a nearby meteorological station was used for times during which temperature or pressure measurements were not reported. As this data was not available for the second day, the diurnal fit of the first experiment's temperature profile was scaled to replace missing values. While temperature and pressure data effect calculated rate constants and therefore modeled HCHO concentrations, they do not affect the comparison between FILIF and Hantzsch measurements.

3 Experiments

The Hantzsch and FILIF inlets were collocated inside the atmospheric simulation chamber SAPHIR. This FEP Teflon-walled chamber has a capacity of approximately 270 m^3. Its retractable roof allows the comparison to take place under either ambient lighting or in dark conditions. Further details on the SAPHIR chamber can be found elsewhere (Rohrer et al., 2005; Wegener et al., 2007; Schlosser et al., 2009).

The filling of the chamber and the addition of HCHO and other species was performed as described in previous intercomparisons detailed by Wisthaler et al. (2008) and Apel et al. (2008), and is briefly described here. The chamber was flushed with high purity synthetic air overnight before each experiment to yield starting conditions with trace gas concentrations below their limit of detection. During the experiments chamber air is diluted as additional synthetic air is added to the chamber to compensate loss from instrument sampling and small leaks in the FEP film. Approximately 2 ppm of methane was added at the start of each experiment to track this dilution. The chamber's mixing fan insured mixing of injected gasses occurred within 2 min.

A summary of each of the four experiments is provided in Table 2. Introduction of HCHO into the chamber was performed either by thermolysis of para-HCHO powder or ozonolysis of 1-butene (C_4H_8). In the first two experiments, a weighted amount of para-HCHO power (Merck; purity > 95 %) was heated in an external glass reactor and swept into the chamber using dry synthetic air. The transfer line was heated to minimize

AMTD
7, 233–255, 2014

wall loss of HCHO. In the second two experiments, C_4H_8 and ozone were injected. To ensure chemical loss of C_4H_8 occurred primarily through reaction with ozone, approximately 500 ppm of CO was injected as an OH-scavenger. Both the thermolysis and ozonolysis methods were repeated under high and low relative humidity conditions (RH > 60 % and < 2 %). Water vapor was injected to the chamber prior to the injection of HCHO or 1-Butene.

4 Model calculations

For all experiments, HCHO mixing ratios were calculated using a modified version of the UW-CAFE model (Wolfe and Thornton, 2011) equipped with MCM v 3.2 chemistry (Jenkin et al., 1997; Saunders et al., 2003) using 3 min time steps. For day 1 and 2 experiments, initial HCHO concentrations were calculated from the known mass of para-HCHO and the chamber volume. For day 3 and 4, O_3 and C_4H_8 measurements were used as model constraints, and CO mixing ratios were calculated from the known injection amount. For all experiments, the dilution rate constant is calculated from the loss rate of methane, which is assumed to be lost only through dilution. Measured HCHO photolysis frequencies were used during periods of exposure to sunlight. Temperature and relative humidity were also used as model inputs.

As described in Sect. 2.3, a lack of temperature and absolute C_4H_8 mixing ratio measurements provide the largest uncertainty in the model calculations. Sensitivity analysis shows a temperature increase of 10 °C results in a 3 % change in calculated HCHO mixing ratios. Adjusting C_4H_8 by 10 % results in approximately 10 % change in HCHO.

5 Results and discussion

For each experiment, we discuss the agreement of the two instruments and the comparison to the model calculations. All time series data are shown in their original time

AMTD
7, 233–255, 2014

base (1 s for FILIF, 11 s for Hantzsch, and 3 min for model). H_2O data is not shown when RH < 2 %. Bivariate least squares regressions were computed following the method of York et al. (2004). Because the Hantzsch instrument inherently measures a 2 min rolling average of HCHO concentrations, the 2 min rolling average of FILIF data is used to provide a comparable measurement for regression analysis. A summary of the regression statistics is provided in Table 3.

5.1 Day 1 (dry conditions, para-HCHO thermolysis)

The results of the thermolysis of para-HCHO under dry chamber conditions are shown in Fig. 1. Calculated HCHO mixing ratios from HCHO injection are higher than both sets of measurements. This possibly could be attributed to insufficient heating of the transfer line resulting in unaccounted wall loss and an overestimate of the initial HCHO mixing ratio, as was seen in Wisthaler et al. (2008).

After injection and until the chamber roof is open at ∼ 09:30 LT, Hantzsch measurements show gradually increasing HCHO, while model calculations and FILIF measurements show a sharp increase followed by a relatively constant concentration. A gradual increase over this 1.5 h time frame is unexpected, as SAPHIR was connected to the addition chamber for ∼ 20 min and the timescale of mixing within the chamber is ∼ 3 min.

Beyond the initial time period, Hantzsch-FILIF agreement was relatively constant. The entire day's correlation is $R^2 = 0.998$. Linear regression of Hantzsch v. FILIF provides a slope of 0.868 ± 0.0002 and an intercept of -0.092 ± 0.001 ppb. The slope falls within the combined FILIF and Hantzsch accuracies (15 % + 5 %). The negative offset can be attributed to instrument zero methods. While the Hantzsch instrument uses air scrubbed of HCHO to determine any instrument offset, the FILIF instrument assumes direct proportionality with fluorescence signal and HCHO mixing ratio. As fluorescence is detected in the sample before the injection of HCHO into the chamber, FILIF measures ∼ 100 ppt in the "clean" air, though Hantzsch reports no HCHO is present.

AMTD
7, 233–255, 2014

5.2 Day 2 (humid conditions, para-HCHO thermolysis)

Figure 2 shows the results of the thermolysis of para-HCHO under humid chamber conditions. Again, incomplete transfer of thermolyzed para-HCHO is suspected to cause calculated HCHO mixing ratios higher than both measurements. FILIF was disconnected from SAPHIR from ~ 14:15–16:30 LT for calibrations. This calibration factor was applied to the entire experiment. FILIF measurements after the calibration show more significant scatter than earlier measurements, as laser power drifted more frequently during this time.

Notably, FILIF HCHO measurements increase during chamber humidification before HCHO injection, while Hantzsch measurements stay constant. Hantzsch measurements on day 4 showed a similar increase in HCHO during chamber humidification (Fig. 4). It is unclear if humidification may lead to an increase in HCHO, and we therefore cannot attribute the increase on day 2 FILIF measurements to a water interference.

The Hantzsch-FILIF relationship seems to differ slightly from the earlier measurements after reconnection to the chamber. Regression analysis over the entire day provides a slope of 1.091 ± 0.0002, a y intercept of -0.246 ± 0.001 ppb, and an R^2 of 0.997. Fitting the earlier measurements provides a slope of 1.06 and a y intercept of 0.04 ppb, while fitting later measurements yields a slope of 0.989 and a y intercept of -0.15 ppb. We conclude the discrepancy between the two time periods is not an artifact of a water interference, but more likely a result of laser drift.

The slopes of each time period as well as the entire data set falls within the stated uncertainty of FILIF. While fitting the entire data set provides a large negative offset, treating the two regimes individually provides y intercepts closer to the anticipated range of -100 to 0 ppt.

5.3 Day 3 (dry conditions, C_4H_8 ozonolysis)

The results of the ozonolysis of C_4H_8 under dry chamber conditions are shown in Fig. 3. Hantzsch measurements are not available after 13:00 LT due to a malfunctioning

AMTD
7, 233–255, 2014

zero valve. The regression analysis provides a slope of 1.132 ± 0.0001, y intercept of -0.338 ± 0.001 ppb, and $R^2 = 0.998$. Except at low (< 400 ppt) and very high (> 20 ppb) concentrations, Hantzsch and FILIF measurements fall within 15 % of each other.

5.4 Day 4 (humid conditions, C_4H_8 ozonolysis)

Figure 4 shows the results of the ozonolysis of C_4H_8 under humid chamber conditions. FILIF measurements are not available before ~ 13:00 LT due to fluctuations in laser power and wavelength not typical during field operation. Regression analysis provides a slope of 0.975 ± 0.0001, y intercept of -0.215 ± 0.001 ppb, and $R^2 = 0.997$. This y intercept is similar to that seen in the day 2 experiment which did not include ozone. The Hantzsch v. FILIF slope falls between the two slopes observed in the dry-conditions experiment. For the two humid conditions experiments, no repeatable systematic offset is observed.

6 Conclusions

Comparison between Hantzsch and FILIF HCHO measurements at the atmosphere simulation chamber SAPHIR demonstrated agreement between the two techniques within 15 % and good correlation ($R^2 \geq 0.997$) under nearly all conditions. At low and very high HCHO concentrations (< 400 ppt and > 20 ppb), the difference between the techniques was at times larger than the 15 % accuracy of the FILIF measurements, but within the combined accuracies of the two techniques.

If water vapor were to significantly decrease the sensitivity of the FILIF instrument due to increased fluorescence quenching, the artifact would manifest itself in systematically lower slopes in Hantzsch v. FILIF during humid experiments. No such trend is discernible, indicating this artifact was not identifiable in this intercomparison. Though the day 2 experiment showed an increasing FILIF-Hantzsch offset with increasing water vapor, this was not observed on the day 4 experiment and remains unexplained.

AMTD
7, 233–255, 2014

An ozone bias for the Hantzsch instrument would yield poor FILIF-Hantzsch agreement for the 1-butene ozonolysis studies. While the dry ozonolysis study had the largest discrepancy from one-to-one agreement and the largest offset, it was unclear which of the instruments involved in this study is more accurate. Furthermore, the humid ozonolysis study resulted in the best instrument agreement (slope = 0.978) and a reasonable *y* intercept considering the different methods of instrument zeroing (−220 ppt). Therefore, we cannot conclude any discrepancies were a result of ozone artifacts.

FILIF and Hantzsch HCHO measurements agree within the stated accuracy over a wide range of experimental conditions. Given the good agreement in previous intercomparisons between the Hantzsch techniques and the PTRMS measurements (Wisthaler et al., 2008), the cause of the factor-of-two disagreement observed between PTR-TOF-MS and FILIF measurements during the BEACHON field campaign is unclear. Possibly, VOCs present during BEACHON-ROCS but not in the SAPHIR intercomparisons could fragment and produce an ion isomeric with HCHO. An intercomparison between these two techniques under controlled chamber conditions could confirm this hypothesis.

Acknowledgements. This material is based upon work supported by the National Science Foundation Graduate Research Fellowship under Grant No. DGE-1256259. The authors also thank the National Science Foundation (AGS 1051338) for support. We acknowledge the inputs from all participants of the intercomparison study. The authors also thank G. M. Wolfe for technical support with the FILIF instrument, R. Häseler for technical support with SAPHIR and B. Bohn for providing photolysis frequencies. The work was supported by T. Brauers and A. Wahner.

References

Ahlm, L., Liu, S. Day, D. A., Russell, L. M., Weber, R., Gentner, D. R., Goldstein, A. H., DiGangi, J. P., Henry, S. B., Keutsch, F. N., VandenBoer, T. C., Markovic, M. Z., Murphy, J. G., Ren, X. R., and Scheller, S.: Formation and growth of ultrafine particles

from secondary sources in Bakersfield, California, J. Geophys. Res., 117, D00V08, doi:10.1029/2011JD017144, 2012.

Apel, E. C., Brauers, T., Koppmann, R., Bandowe, B., Bossmeyer, J., Holzke, C., Tillmann, R., Wahner, A., Wegener, R., Brunner, A., Jocher, M., Ruuskanen, T., Spirig, C., Steigner, D., Steinbrecher, R., Alvarez, E. G., Mueller, K., Burrows, J. P., Schade, G., Solomon, S. J., Ladstaetter-Weissenmayer, A., Simmonds, P., Young, D., Hopkins, J. R., Lewis, A. C., Legreid, G., Reimann, S., Hansel, A., Wisthaler, A., Blake, R. S., Ellis, A. M., Monks, P. S., and Wyche, K. P.: Intercomparison of oxygenated volatile organic compound measurements at the SAPHIR atmosphere simulation chamber, J. Geophys. Res., 113, D20307, doi:10.1029/2008JD009865, 2008.

Dasgupta, P. K., Li, J. Z., Zhang, G. F., Luke, W. T., McClenny, W. A., Stutz, J., and Fried, A.: Summertime ambient formaldehyde in five US metropolitan areas: Nashville, Atlanta, Houston, Philadelphia, and Tampa, Environ. Sci. Technol., 39, 4767–4783, doi:10.1021/es048327d, 2005.

DiGangi, J. P., Boyle, E. S., Karl, T., Harley, P., Turnipseed, A., Kim, S., Cantrell, C., Maudlin III, R. L., Zheng, W., Flocke, F., Hall, S. R., Ullmann, K., Nakashima, Y., Paul, J. B., Wolfe, G. M., Desai, A. R., Kajii, Y., Guenther, A., and Keutsch, F. N.: First direct measurements of formaldehyde flux via eddy covariance: implications for missing in-canopy formaldehyde sources, Atmos. Chem. Phys., 11, 10565–10578, doi:10.5194/acp-11-10565-2011, 2011.

DiGangi, J. P., Henry, S. B., Kammrath, A., Boyle, E. S., Kaser, L., Schnitzhofer, R., Graus, M., Turnipseed, A., Park, J-H., Weber, R. J., Hornbrook, R. S., Cantrell, C. A., Maudlin III, R. L., Kim, S., Nakashima, Y., Wolfe, G. M., Kajii, Y., Apel, E.C., Goldstein, A. H., Guenther, A., Karl, T., Hansel, A., and Keutsch, F. N.: Observations of glyoxal and formaldehyde as metrics for the anthropogenic impact on rural photochemistry, Atmos. Chem. Phys., 12, 9529–9543, doi:10.5194/acp-12-9529-2012, 2012.

Heard, D. E.: Analytical Techniques for Atmospheric Measurement, Blackwell Publishing, Oxford, UK, ISBN 1405123575, 2006.

Hottle, J. R., Huisman, A. J., Digangi, J. P., Kammrath, A., Galloway, M. M., Coens, K. L., and Keutsch, F. N.: A laser induced fluorescence-based instrument for in-situ measurements of atmospheric formaldehyde, Environ. Sci. Technol., 43, 790–795, doi:10.1021/es801621f, 2009.

AMTD
7, 233–255, 2014

Jenkin, M. E., Saunders, S. M., Wagner, V., and Pilling, M. J.: Protocol for the development of the Master Chemical Mechanism, MCM v3 (Part B): tropospheric degradation of aromatic volatile organic compounds, Atmos. Chem. Phys., 3, 181–193, doi:10.5194/acp-3-181-2003, 2003.

Kaser, L., Karl, T., Schnitzhofer, R., Graus, M., Herdlinger-Blatt, I. S., DiGangi, J. P., Sive, B., Turnipseed, A., Hornbrook, R. S., Zheng, W., Flocke, F. M., Guenther, A., Keutsch, F. N., Apel, E., and Hansel, A.: Comparison of different real time VOC measurement techniques in a ponderosa pine forest, Atmos. Chem. Phys., 13, 2893–2906, doi:10.5194/acp-13-2893-2013, 2013.

Kelly, T. J. and Fortune, C. R.: Continuous monitoring of gaseous formaldehyde using an improved fluorescence approach, Int. J. Environ. An. Ch., 54, 249–263, doi:10.1080/03067319408034093, 1994.

Krinke, S.: Experimentelle Bestimmung der Depositionsgeschwindigkeit von Formaldehyd und Ozon über einem Laubwaldbestand, Ph.D. thesis, Universität Stuttgart, 1999.

Li, X., Rohrer, F., Brauers, T., Häseler, R., Hofzumahaus, A., Bohn, B., Broch, S., Fuchs, H., Gomm, S., Holland, F., Jäger, J., Kaiser, J., Keutsch, F. N., Lohse, I., Lu, K., Tillmann, R., Wegener, R.,Wolfe, G. M., Mentel, T. F., Kiendler-Scharr, A., and Wahner, A.: Photo-induced formation of nitrous acid from a gas-phase volume source in the troposphere, in review, 2014.

Rohrer, F., Bohn, B., Brauers, T., Brüning, D., Johnen, F.-J., Wahner, A., and Kleffmann, J.: Characterisation of the photolytic HONO-source in the atmosphere simulation chamber SAPHIR, Atmos. Chem. Phys., 5, 2189–2201, doi:10.5194/acp-5-2189-2005, 2005.

Saunders, S. M., Jenkin, M. E., Derwent, R. G., and Pilling, M. J.: Protocol for the development of the Master Chemical Mechanism, MCM v3 (Part A): tropospheric degradation of non-aromatic volatile organic compounds, Atmos. Chem. Phys., 3, 161–180, doi:10.5194/acp-3-161-2003, 2003.

Schlosser, E., Brauers, T., Dorn, H.-P., Fuchs, H., Häseler, R., Hofzumahaus, A., Holland, F., Wahner, A., Kanaya, Y., Kajii, Y., Miyamoto, K., Nishida, S., Watanabe, K., Yoshino, A., Kubistin, D., Martinez, M., Rudolf, M., Harder, H., Berresheim, H., Elste, T., Plass-Dülmer, C., Stange, G., and Schurath, U.: Technical Note: Formal blind intercomparison of OH measurements: results from the international campaign HOxComp, Atmos. Chem. Phys., 9, 7923–7948, doi:10.5194/acp-9-7923-2009, 2009.

AMTD
7, 233–255, 2014

Seinfeld, J. H. and Pandis, S. N.: Atmospheric Chemistry and Physics from Air Pollution to Climate Change, 2nd Edn., John Wiley and Sons, available at http://www.knovel.com/web/portal/browse/display?_EXT_KNOVEL_DISPLAY_bookid=2126&VerticalID=0, 2006.

Vlasenko, A., Macdonald, A .M., Sjostedt, S. J., and Abbatt, J. P. D.: Formaldehyde measurements by Proton transfer reaction – Mass Spectrometry (PTR-MS): correction for humidity effects, Atmos. Meas. Tech., 3, 1055–1062, doi:10.5194/amt-3-1055-2010, 2010.

Warneke, C., Veres, P., Holloway, J. S., Stutz, J., Tsai, C., Alvarez, S., Rappenglueck, B., Fehsenfeld, F. C., Graus, M., Gilman, J. B., and de Gouw, J. A.: Airborne formaldehyde measurements using PTR-MS: calibration, humidity dependence, inter-comparison and initial results, Atmos. Meas. Tech., 4, 2345–2358, doi:10.5194/amt-4-2345-2011, 2011.

Wegener, R., Brauers, T., Koppmann, R., Rodríguez Bares, S., Rohrer, F., Tillmann, R., Wahner, A., Hansel, A., and Wisthaler, A.: Investigation of the ozonolysis of short chained alkenes in the atmosphere simulation chamber SAPHIR, J. Geophys. Res., 112, D13301, doi:10.1029/2006JD007531, 2007.

Wert, B. P., Fried, A., Henry, B., and Cartier, S.: Evaluation of inlets used for the airborne measurement of formaldehyde, J. Geophys. Res.-Atmos., 107, 4163, doi:10.1029/2001jd001072, 2002.

Wisthaler, A., Apel, E. C., Bossmeyer, J., Hansel, A., Junkermann, W., Koppmann, R., Meier, R., Müller, K., Solomon, S. J., Steinbrecher, R., Tillmann, R., and Brauers, T.: Technical Note: Intercomparison of formaldehyde measurements at the atmosphere simulation chamber SAPHIR, Atmos. Chem. Phys., 8, 2189–2200, doi:10.5194/acp-8-2189-2008, 2008.

Wolfe, G. M. and Thornton, J. A.: The Chemistry of Atmosphere-Forest Exchange (CAFE) Model – Part 1: Model description and characterization, Atmos. Chem. Phys., 11, 77–101, doi:10.5194/acp-11-77-2011, 2011.

York, D., Evensen, N. M., Marinez, M. L., and Delgado, J. D. B.: Unified equations for the slope, intercept, and standard errors of the best straight line, Am. J. Phys., 72, 367–375, doi:10.1119/1.1632486, 2004.

AMTD
7, 233–255, 2014

Table 1. Additional measurements accompanying the HCHO intercomparison.

Species	Technique	Accuracy	1σ Precision
O_3	UV Absorption (Ansyco O342M)	3 %	1 ppb
H_2O	Cavity Ring-Down Spectroscopy (Picarro G2301)	0.02 %	< 0.02 %
1-Butene	Proton-Transfer-Reaction Mass Spectrometry	8 %	3–4 %
CH_4	Cavity Ring-Down Spectroscopy (Picarro G2301)	< 1 ppb	< 1 ppb
j_{HCHO}	Spectral Radiometer	10 %	1 %

AMTD
7, 233–255, 2014

Table 2. Description of experimental conditions.

Experiment	HCHO source	Max RH (%)	Periods of Illumination (LT)	Other Injected Species
Day 1	Thermolysis of 3.80 mg para-HCHO	2.0	9:35–10:20; 12:30–13:31	CH_4 (2.08 ppm)
Day 2	Thermolysis of 3.51 mg para-HCHO	69.5	10:28–11:36	CH_4 (2.15 ppm)
Day 3	72.8 ppb C_4H_8 + 200 ppb O_3	0.6	–	CH_4 (2.50 ppm) CO (500 ppm)
Day 4	24.3 ppb C_4H_8 + 485 ppb O_3	79.4	–	CH_4 (2.03 ppm) CO (500 ppm)

AMTD
7, 233–255, 2014

Table 3. Linear correlations for Hantzsch v. FILIF measurements calculated with a 95 % confidence interval.

Experiment	Slope (Hantzsch/FILIF)	Intercept (ppb)	Correlation (R^2)
Day 1	0.868 ± 0.0002	-0.092 ± 0.001	0.998
Day 2	1.091 ± 0.0002	-0.246 ± 0.001	0.997
Day 3	1.132 ± 0.0001	-0.338 ± 0.001	0.998
Day 4	0.975 ± 0.0001	-0.215 ± 0.001	0.997

AMTD
7, 233–255, 2014

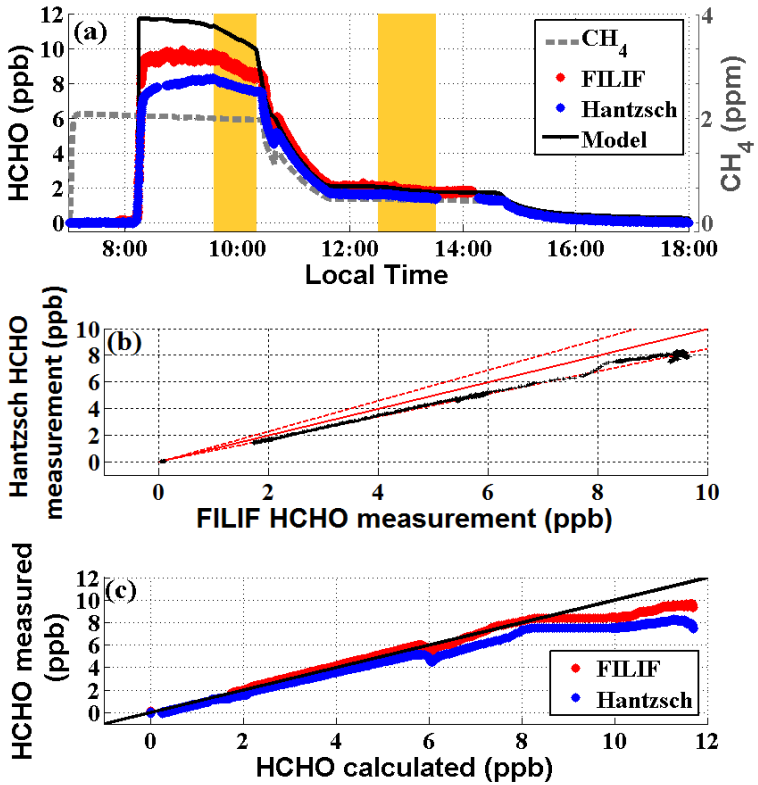

Fig. 1. (a) Time series of measured and calculated HCHO mixing ratios as well as the dilution tracer (CH_4) during day 1, with periods of illumination denoted by yellow panels. **(b)** Comparison between HCHO measurements. Error bars represent 3σ precision. Lines represent one-to-one agreement and ±15 % FILIF measurements. **(c)** Measurement/model comparison, with the line showing 1–1 agreement.

AMTD
7, 233–255, 2014

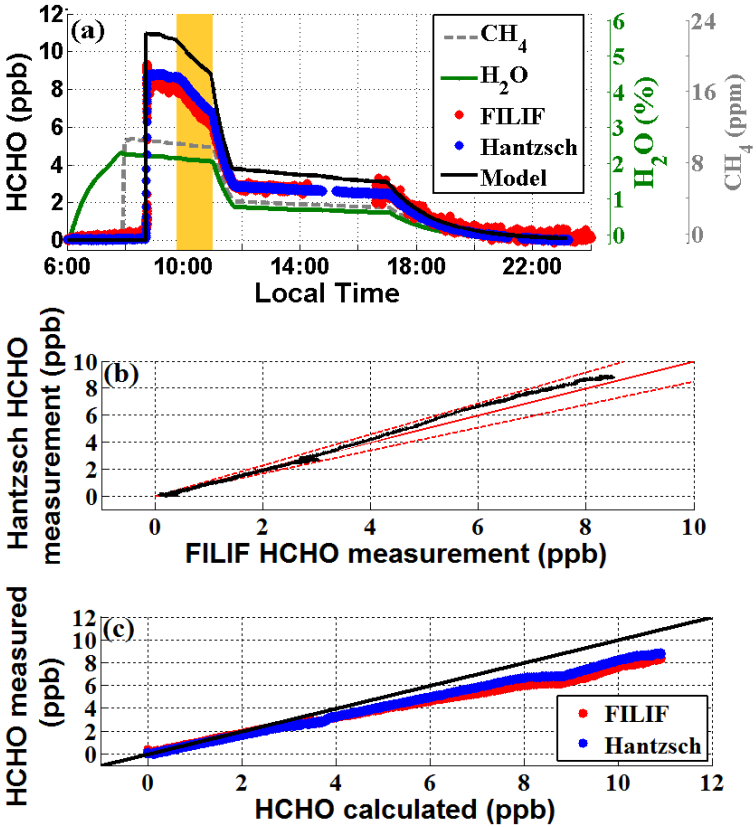

Fig. 2. (a) Time series of measured and calculated HCHO mixing ratios, CH_4, and H_2O during day 2, with periods of illumination denoted by yellow panels. **(b)** Comparison between HCHO measurements. Error bars represent 3σ precision. Lines represent one-to-one agreement and ±15 % FILIF measurements. **(c)** Measurement/model comparison, with the line showing 1–1 agreement.

AMTD
7, 233–255, 2014

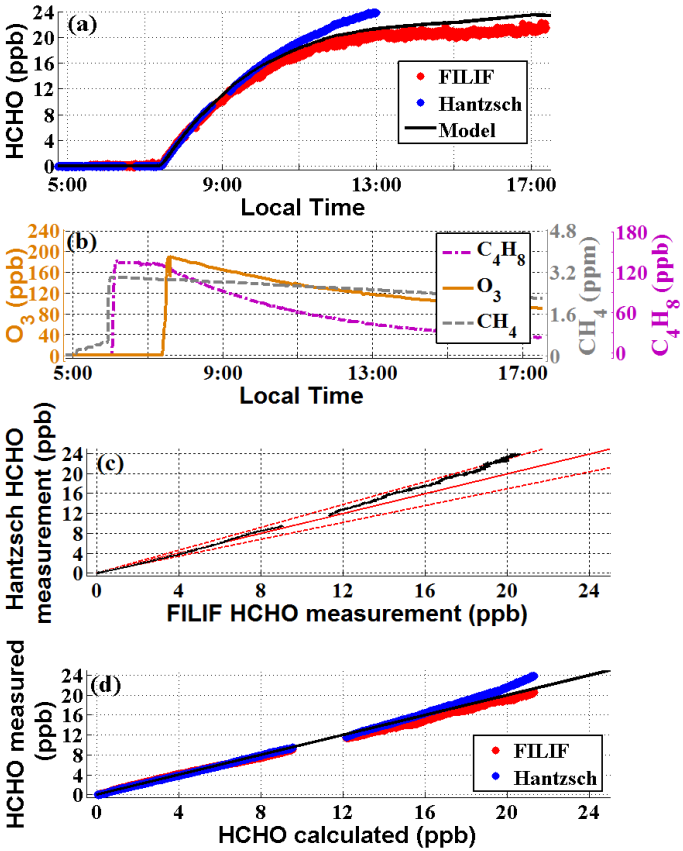

Fig. 3. (a) Time series of measured and calculated HCHO mixing ratios during day 3. **(b)** Time series of C_4H_8, ozone, and CH_4. **(c)** Comparison between HCHO measurements. Error bars represent 3σ precision. Lines represent one-to-one agreement and ±15 % FILIF measurements. **(d)** Measurement/model comparison, with the line showing 1–1 agreement.

AMTD
7, 233–255, 2014

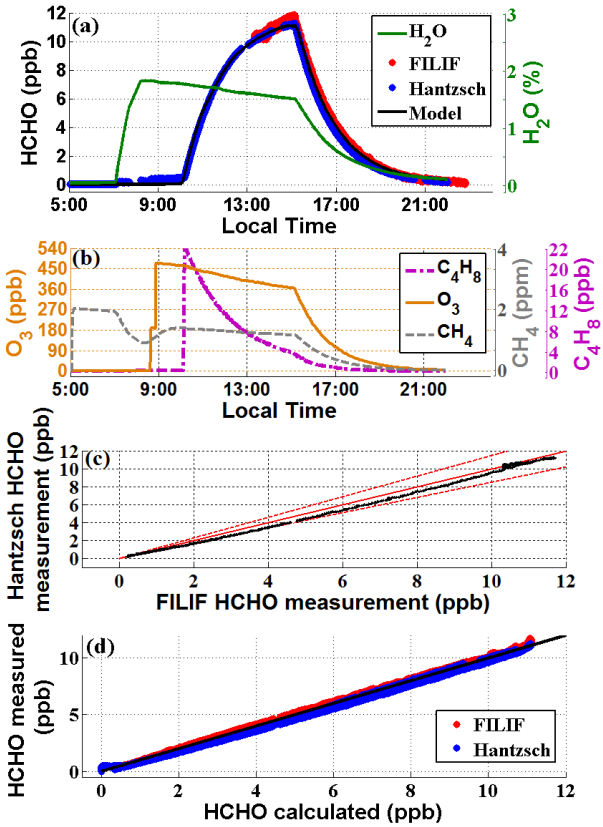

Fig. 4. (a) Time series of measured and calculated HCHO mixing ratios and H_2O during day 4. **(b)** Time series of C_4H_8, ozone, CH_4. **(c)** Comparison between HCHO measurements. Error bars represent 3σ precision. Lines represent one-to-one agreement and ±15 % FILIF measurements. **(d)** Measurement/model comparison, with the line showing 1–1 agreement.

AMTD
7, 233–255, 2014